


Journal of Geophysical Research: Atmospheres / Volume 115, Issue D10

Aerosol and Clouds | [Free Access](#)

## In situ and lidar observations of tropopause subvisible cirrus clouds during TC4

Sean Davis , Dennis Hlavka, Eric Jensen, Karen Rosenlof, Qiong Yang, Sebastian Schmidt, Stephan Borrmann, Wiebke Frey, Paul Lawson, Holger Voemel, T. P. Bui

First published: 10 September 2010

<https://doi.org/10.1029/2009JD013093>

Cited by: 22

### Abstract

[1] During the Tropical Composition, Clouds, and Climate Coupling (TC4) experiment in July–August 2007, the NASA WB-57F and ER-2 aircraft made coordinated flights through a tropopause subvisible cirrus (SVC) layer off the Pacific Coast of Central America. The ER-2 aircraft was equipped with a remote sensing payload that included the cloud physics lidar (CPL). The WB-57F payload included cloud microphysical and trace gas measurements, and the aircraft made four vertical profiles through the SVC layer shortly after the ER-2 flew over. The in situ and remotely sensed data are used to quantify the meteorological and microphysical properties of the SVC layer, and these data are compared to the limited set of SVC measurements that have previously been made. It is found that the layer encountered was particularly tenuous, with optical depths ( $\tau$ ) between about  $10^{-4}$  and  $10^{-3}$ . From the in situ and other meteorological data, radiative heating rate perturbations of  $\sim 0.05$ – $0.1$  K day $^{-1}$  are calculated. These heating rates are smaller than previous estimates for tropopause SVC, consistent with the smaller  $\tau$  in the present study. Coverage statistics based on CPL data from other TC4 flights indicate that this cloud was not an outlier among the sampled population. SVC with properties similar to the one presented here are below the detection limit of space-based lidars such as CALIPSO, and a comparison with the TC4 statistics suggests that a majority (>50%) of tropopause SVC (with  $\tau < 0.01$ ) could be unaccounted for in studies using CALIPSO data.

### 1. Introduction

[2] Cirrus clouds play an important role in Earth's radiative energy balance, and may contribute either a positive or negative radiative effect depending on their microphysical properties [e.g., [Fu and Liou, 1993](#); [Stephens et al., 1990](#)]. Within the broader category of cirrus clouds, subvisible cirrus clouds (SVC) with optical depths ( $\tau$ ) less than  $\sim 0.03$  have been found to have a

net positive radiative effect on the top-of-atmosphere energy budget due to their infrared “greenhouse” effect outweighing their solar “albedo” effect [[Comstock et al., 2002](#); [Fu and Liou, 1993](#); [McFarquhar et al., 2000](#)]. Similarly, thin cirrus ( $\tau < 0.3$ ), which include SVC, have been estimated to make a significant contribution to the global top-of-atmosphere (TOA) radiation budget through their reduction of outgoing longwave radiation (OLR) [[Haladay and Stephens, 2009](#)].

[3] In this paper, we discuss aircraft measurements of a distinct class of SVC that have recently been referred to as ultrathin tropical tropopause clouds (UTTCs) [[Luo et al., 2003a, 2003b](#); [Peter et al., 2003](#)]. We use tropopause SVC (or simply SVC) here as a label for laminar clouds that have presumably formed in situ near the tropical tropopause, as opposed to cirrus clouds that are associated with recent outflow from convection [[Comstock et al., 2002](#); [Pfister et al., 2001](#)]. Note that most of these clouds will qualify as being subvisual based on their optical depth ( $\tau < 0.03$ ) [[Sassen et al., 1989](#)], but clouds with larger optical depths are not excluded from this analysis.

[4] In addition to their radiative importance, tropopause SVC are likely involved in dehydration and radiative heating of air as it ascends through the tropical uppermost troposphere into the stratosphere [[Corti et al., 2006](#); [Jensen et al., 1996a](#); [Luo et al., 2003a](#)], thereby affecting the rates of transport of chemical constituents from convective detrainment levels up to the stratosphere. SVC may also impact tropical tropopause temperatures and play a role in regulating the humidity of air entering the stratosphere [[Rosenfield et al., 1998](#)], which in turn affects the radiative budget [[Forster and Shine, 2002](#)] and stratospheric ozone chemistry [[Dvortsov and Solomon, 2001](#)].

[5] Compared to other cloud types, very few in situ measurements have been made of SVC in part because of their high altitudes ( $>15$  km) that necessitate the use of specialized high-altitude research aircraft. As such, the microphysical and radiative properties of these clouds are not well constrained. The only known in situ SVC measurements at the time of writing are from the tropical Western Pacific in December 1973 [[Heymsfield and Jahnsen, 1974](#); [Heymsfield, 1986](#); [McFarquhar et al., 2000](#)], the Indian Ocean during APE-THESEO in February and March 1999 [[Luo et al., 2003a](#); [Thomas et al., 2002](#)], tropical West Africa during the AMMA campaign, and the tropical Eastern Pacific during CR-AVE in 2006 [[Lawson et al., 2008](#)]. The SVC measurements presented below were taken in the same region as those from CR-AVE, except that these measurements were taken in July and August when the tropopause was relatively warm ( $\sim 200$  K), as opposed to January and February for CR-AVE when the tropopause was very cold ( $\sim 190$  K).

[6] Overall, the previous in situ measurements of SVC indicate relatively consistent microphysical properties, with thicknesses  $\sim 100$ – $1$  km, ice concentrations  $\sim 10$ – $100$  L<sup>-1</sup>, particle

effective radii  $\sim 10\text{--}20\ \mu\text{m}$ , extinctions  $\sim 10^{-4}\text{--}10^{-3}\ \text{km}^{-1}$ , and ice water content (IWC)  $10^{-4}\text{--}10^{-3}\ \text{g m}^{-3}$  ( $\sim 0.1\text{--}1\ \text{ppmv}$ ). However, there have been some notable differences in SVC microphysical properties among the limited set of in situ measurements. For example, [Lawson et al. \[2008\]](#) found during CR-AVE that SVC in the Eastern Pacific were comprised of significantly different ice crystal habits than the Western Pacific SVC observed in 1973. The CR-AVE ice crystals were primarily quasi-spherical, whereas the W. Pacific SVC contained mostly columnar and trigonal plates. Furthermore, the Eastern Pacific SVC were also found to contain crystals larger than  $50\ \mu\text{m}$ , which did not exist in the W. Pacific data set. Although differences due to measurement technique can not be ruled out, the differences in crystal habit between the CR-AVE and previous SVC measurements bring up the possibility that geographic, seasonal, and/or long-term (i.e., climate change-related) differences in the microphysical properties of SVC exist [[Lawson et al., 2008](#)]. Also, the presence of relatively large ice crystals calls into question some of the formation mechanisms needed for these clouds [[Jensen et al., 2008](#)].

[7] In this paper, we present a case study involving coordinated in situ and remote-sensing SVC measurements from the NASA ER-2 and WB-57F aircraft taken during the Tropical Composition, Clouds, and Climate Coupling (TC4) experiment in August 2007. The subvisible cirrus data presented in this paper represent a unique set of measurements that allow us to assess the microphysical and radiative properties of this cloud. In the next section, we present the in situ and remote sensing data from this SVC cloud encounter. The in situ microphysical data are compared to previous in situ measurements in tropical tropopause SVC. Then, radiative heating rate and cloud radiative forcing calculations are presented. Finally, aircraft-based lidar data are used to provide regional coverage statistics for SVC in the equatorial Eastern Pacific during the TC4 campaign, and these data are compared with other aircraft and satellite-based climatologies.

## 2. SVC Observations From 6 August 2007 TC4 Flights

[8] The Tropical Composition, Clouds and Climate Coupling (TC4) experiment was based out of San Jose, Costa Rica during July and August 2007 [[Toon et al., 2010](#)]. Three NASA research aircraft took part in this mission: the NASA DC-8 (low- to mid-troposphere), the WB-57F (TTL region), and the ER-2 (lower stratosphere). The DC-8 and WB-57F were equipped with in situ and remote sensing measurements, whereas the ER-2 contained a remote sensing payload that included the “A-train” simulator instruments such as the Moderate Resolution Imaging Spectroradiometer (MODIS) airborne simulator (MAS) and the Cloud Physics Lidar (CPL) [[McGill et al., 2002](#)].

[9] Throughout TC4, various combinations of these aircraft flew along coordinated tracks for the purposes of providing a complete set of measurements of the chemical, microphysical, and radiative environment. This paper focuses on one such flight from 6 August in which the three

aircraft flew along a NE-SW flight leg from San Jose, Costa Rica towards the Galapagos Islands (see [Figure 1](#)).

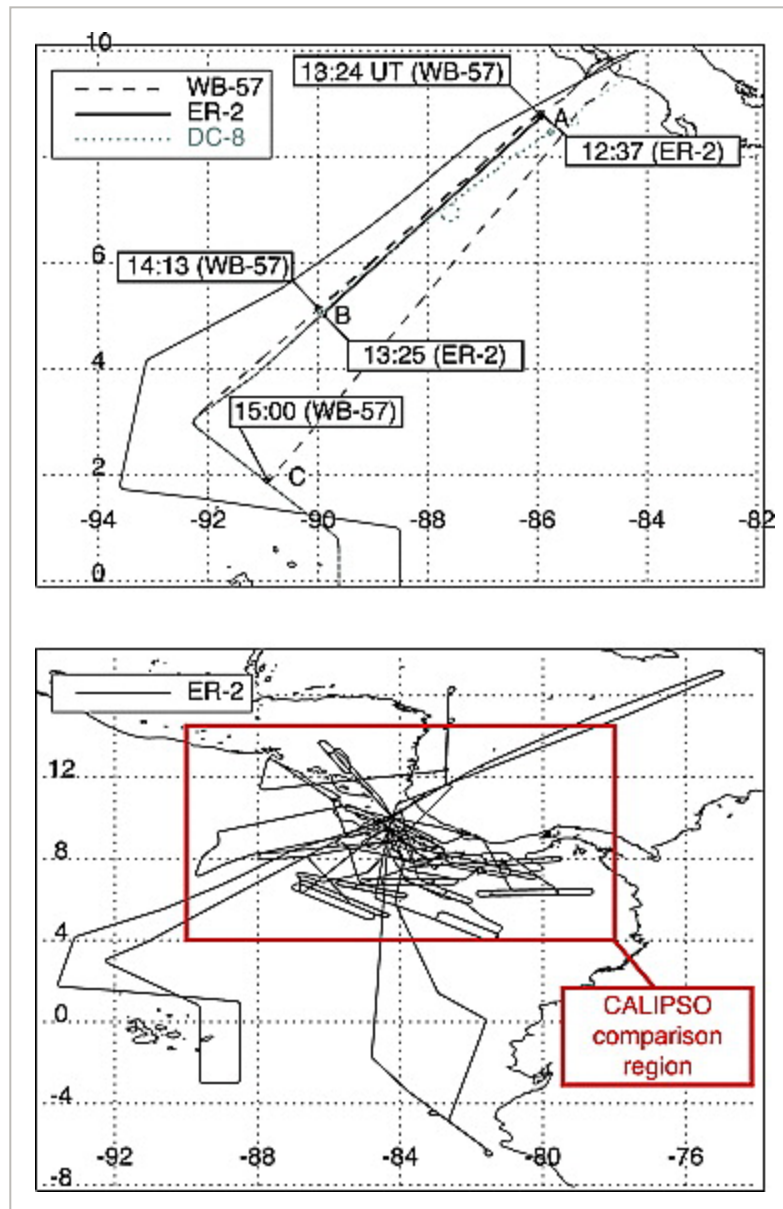


**Figure 1**

[Open in figure viewer](#) | [PowerPoint](#)

(top) The WB-57F and ER-2 flight tracks on 6 August 2007. Both planes flew along segment AB during their outbound legs, with the WB-57F lagging about 45 minutes behind the ER-2. Along segment BC, the WB-57F porpoised and sampled clear air near the tropopause. (bottom) ER-2 flight tracks for all 11 TC-4 flights based out of San Jose, Costa Rica, along with a box around the region from which the histograms in [Figure 9](#) are based.



[10] On this day, the ER-2 flew outbound from San Jose, Costa Rica, and a tropopause SVC layer was observed at ~16.5 km from ~12:45–13:15 UT in the preliminary CPL data that was transmitted to the mission operations facility in real time. This allowed the mission scientists to direct the WB-57F to the SVC layer approximately 45 minutes afterwards, where it performed several up-and-down “porpoise” maneuvers, ultimately making four passes through the SVC layer.

[11] Measurements used in this study that were made from the WB-57F include water vapor, cloud microphysical, and meteorological data. Water vapor data used here are from the JPL Laser Hygrometer (JLH), which has a stated accuracy of  $\pm 10\%$  ( $1\sigma$ ) [May, 1998] and Harvard Lyman- $\alpha$  photofragment fluorescence hygrometer (HW), which has a stated accuracy of  $\pm 5\%$  ( $1\sigma$ ) [Hintsa et al., 1999; Weinstock et al., 1994, 2009]. Pressure and temperature measurements with an accuracy of  $\pm 0.25$  hPa and  $\pm 0.25$  K, respectively, are provided by the meteorological measurement system (MMS) [Scott et al., 1990].

[12] Cloud microphysical data are from the Cloud Particle Imager (CPI) [Lawson et al., 2001] and 2D-S [Lawson et al., 2006]. Here, we use the CPI to provide ice crystal habit information based on images of particles larger than  $10 \mu\text{m}$  ( $2.3 \mu\text{m}$  pixel resolution). Ice crystal size distributions from  $10 \mu\text{m}$ – $8 \text{mm}$  are provided by the 2D-S, which images particles with  $10 \mu\text{m}$  resolution. The 2D-S image data are processed as in the work of Lawson et al. [2008] using the Korolev algorithm for resizing out-of-focus images [Korolev, 2007].

[13] Using the total projected particle area ( $A_c$ ) from the 2D-S, visible extinction coefficients ( $\beta_{\text{ext}}$ ) are calculated under the geometric optics assumption (i.e.,  $2\pi r/\lambda \gg 1$  and  $Q_{\text{ext}} = 2$ ). To estimate IWC, the mass as a function of area relationship from Baker and Lawson [2006] is used for particles larger than  $\sim 50 \mu\text{m}$ , whereas spherical particles are assumed for sizes smaller than  $50 \mu\text{m}$ . Effective radii ( $r_e$ ) are then calculated using IWC and  $A_c$  as in the work of Fu [1996, equation 3.11].

[14] There are several sources of both random and bias error that are likely to affect the cloud microphysical values calculated from 2D-S data, but no quantitative estimates exist for the 2D-S size distributions or quantities derived from them. Potential sources of uncertainty include counting statistics, sample volume uncertainties, image resizing, the particle mass-dimensional relationships (i.e.,  $\text{IWC}(A_c)$ ), and ice crystal shattering on aircraft and instrument surfaces. For the SVC data presented here, the IWC values are 13% less, on average, than IWC calculated assuming spherical particles. The values of  $r_e$  presented here are also correspondingly lower than if they had been calculated with an IWC based on the spherical particle assumption. In general, shattered ice crystals have the potential to contaminate size distributions and derived quantities from particle probe measurements, but the geometry of the 2D-S probe arms, the application of time-of-arrival filtering, the low concentrations of large ice crystals ( $< \sim 10^{-4} \text{L}^{-1}$

with length  $>100 \mu\text{m}$ ) in this case, and previous analysis [[Jensen et al., 2009, 2010](#); [Lawson et al., 2008](#)] indicate that it is very unlikely that the SVC data presented here are contaminated by ice crystal shattering.

[15] An overview time series plot of the ER-2 CPL and WB-57F microphysical and meteorological measurements is shown in [Figure 2](#). [Figures 2a](#) and [2b](#) show the ER-2 CPL lidar 532 nm attenuated backscatter and extinction retrieval data along the flight segment AB identified in [Figure 1](#), with the WB-57F altitude overlotted (red) at the closest (lat/lon) location to the ER-2. [Figures 2c–2g](#) show the in situ data from the WB-57F taken along the same segment approximately an hour after the ER-2.

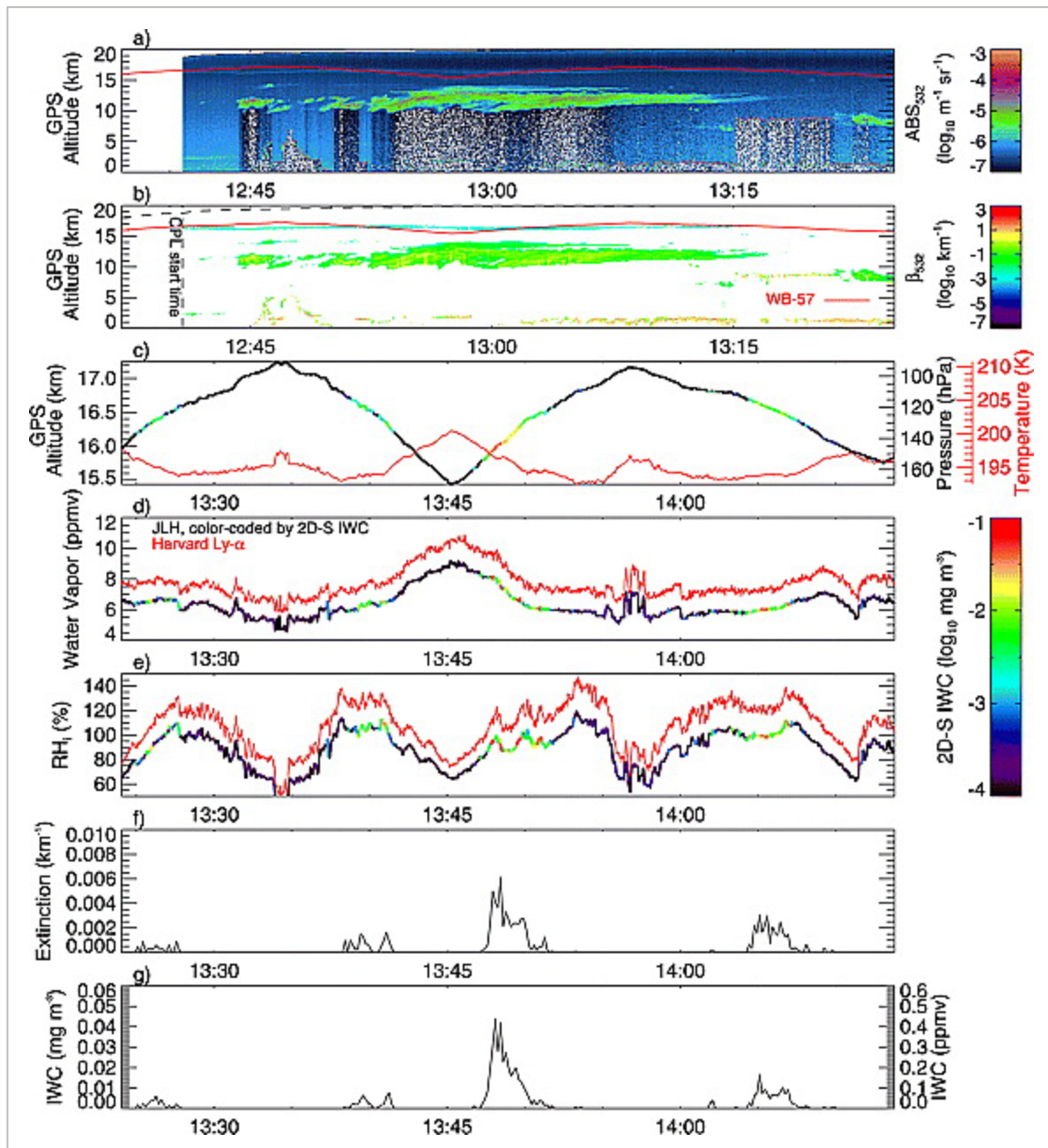


**Figure 2**

[Open in figure viewer](#) | [PowerPoint](#)

Time series plots of subvisible cirrus measurements taken during the 6 August 2007 TC4 ER-2 and WB-57F flights, plotted along the segment AB shown in [Figure 1](#). Data are the (a and b) ER-2 CPL attenuated backscatter (ABS) and extinction at 532 nm ( $\beta_{532}$ ), (c) in situ temperature and altitude from the WB-57F MMS (altitude color-coded by 2D-S IWC), (d and e) water vapor and RH<sub>i</sub> from the JLH and Harvard instruments on the WB-57F, and (f and g) visible optical extinction and ice water content from the 2D-S on the WB-57F.

[16] As shown in [Figure 2](#), the SVC layer is present in the CPL backscatter data from ~12:40–13:15 UT, which corresponds to a horizontal distance of 440 km. The ER-2 CPL data and WB-57F in situ measurements indicate that the SVC layer was extremely tenuous, with mean values of 2 L<sup>-1</sup> (2D-S number concentration, N<sub>i</sub>), 0.001 km<sup>-1</sup> (2D-S  $\beta_{\text{ext}}$ ), 0.00064 (CPL  $\tau$ ), 14  $\mu\text{m}$  (2D-S  $r_e$ ), and  $5.6 \times 10^{-6}$  g m<sup>-3</sup> (2D-S IWC). For comparison, the mean values from CR-AVE reported by [Lawson et al. \[2008\]](#) are 66 L<sup>-1</sup> (N<sub>i</sub>), 0.009 km<sup>-1</sup> ( $\beta_{\text{ext}}$ ), 0.068 ( $\tau$ ), 8.8  $\mu\text{m}$  ( $r_e$ ) and  $5.5 \times 10^{-5}$  g m<sup>-3</sup> (IWC).

[17] As shown in [Figure 2](#), the in-cloud water vapor values are in the range of 6–10 ppmv, with relative humidity with respect to ice (RH<sub>i</sub>) ~ 80–130%, depending on the instrument used. For the four passes through the SVC layer, the mean JLH RH<sub>i</sub> is 98%, whereas the mean HW value is 120%. For each instrument, the in-cloud water vapor values span a range of slightly more than 2 ppmv, and the mean offset between the two instruments (HW-JLH) is 1.3 ppmv. At sub-10 ppmv WV mixing ratios, similar offsets have been noted between HW and other WV measurements, and these offsets are well outside of the combined instrumental uncertainties [e.g., [Gensch et al., 2008](#); [Kley et al., 2000](#); [Vömel et al., 2007](#); [Weinstock et al., 2009](#)]. Nevertheless, neither instrument observed large RH<sub>i</sub> (i.e., >~160%) in these SVC, in contrast with the CR-AVE measurements where supersaturations of ~200% were noted inside SVC by the HW and the Harvard ICOS instruments [[Gensch et al., 2008](#); [Jensen et al., 2008](#); [Lawson et al., 2008](#)]. This difference may reflect the fact that the TC4 SVC were warmer than during CR-AVE (193–198 K as opposed to <190 K for CR-AVE), and there is a well-documented increase in the frequency of observed supersaturation as temperature decreases for temperatures below 200 K [[Gao et al., 2004](#); [Krämer et al., 2009](#)].

[18] [Figure 3](#) shows in situ vertical profiles of the four passes through the SVC layer, as well as the range of values for four additional porpoises made by the WB-57F through clear air immediately following the SVC sampling. The temperature, IWC, and  $\beta_{\text{ext}}$  profiles show that the top of the SVC layer lies immediately below the cold-point tropopause (within ~0–200 m), with the cold-point tropopause defined here as the level of minimum temperature in a vertical profile. That SVC reside near the cold-point has been recognized by previous studies, but their proximity to the cold-point has not been illustrated as clearly as in the case presented here. This property is relevant to the dehydration potential of these types of clouds, and suggests



that if irreversible dehydration is occurring in these clouds, it is likely the last occurrence before the air ascends into the stratosphere.

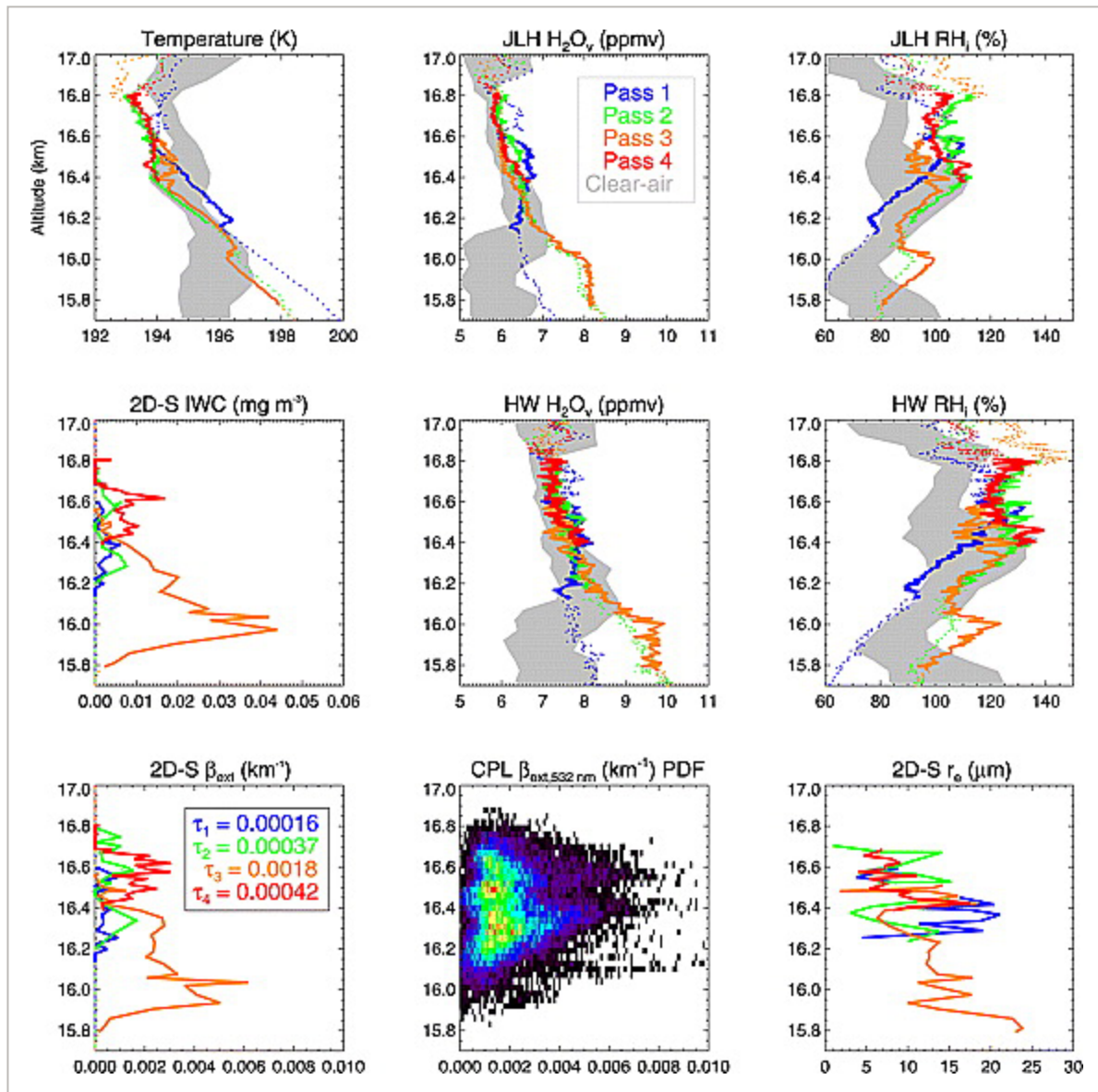


**Figure 3**

[Open in figure viewer](#) | [PowerPoint](#)

Vertical profiles taken from the four passes made through the subvisible cirrus layer on 6 August 2007 by the WB-57F, and CPL data from the ER-2. Thick solid lines are in-cloud data, and dotted lines are clear-air data. All profiles are color-coded by the pass number through the SVC layer, except for the CPL data from the ER-2, which are presented as a 2D probability distribution function.

[19] The vertical profiles also illustrate several salient features of the SVC. First, they are clearly associated with a region of the atmosphere that is high in relative humidity and of limited



vertical extent. In [Figure 3](#), both the JLH and HW instruments indicate that the SVC reside in a region of the atmosphere that is at or above supersaturation, with subsaturated regions below cloud and a limited region of saturation just above cloud. The vertical thickness of the SVC layer ranges from ~300–800 m, with an average of 500 m for the four passes. Another interesting feature in [Figure 3](#) is that there is an overall decrease with height of effective radius, although pass #3 is the only individual leg that clearly shows this relationship. This behavior is expected when the time scale for gravitational size sorting is less than the cloud lifetime. Also, both [Figures 2](#) and [3](#) illustrate that there is considerable horizontal heterogeneity of the SVC layer, with peak extinctions and  $\tau$  for the various passes spanning almost an order of magnitude.

[20] There are also interesting differences in [Figure 3](#) between the clear-air data and the in-cloud data. Individually, each WV instrument indicates very similar values of mixing ratio in cloudy and clear air. However, the temperature is lower in cloud than in clear air, and this explains the higher relative humidity in cloud.

[21] Finally, CPI imagery from the SVC encounters is shown in [Figure 4](#). These images are almost entirely quasi-spherical, similar to the CR-AVE CPI data [[Lawson et al., 2008](#)], but different from the complex columnar and trigonal shapes observed in the Western Pacific by [Heymsfield \[1986\]](#).

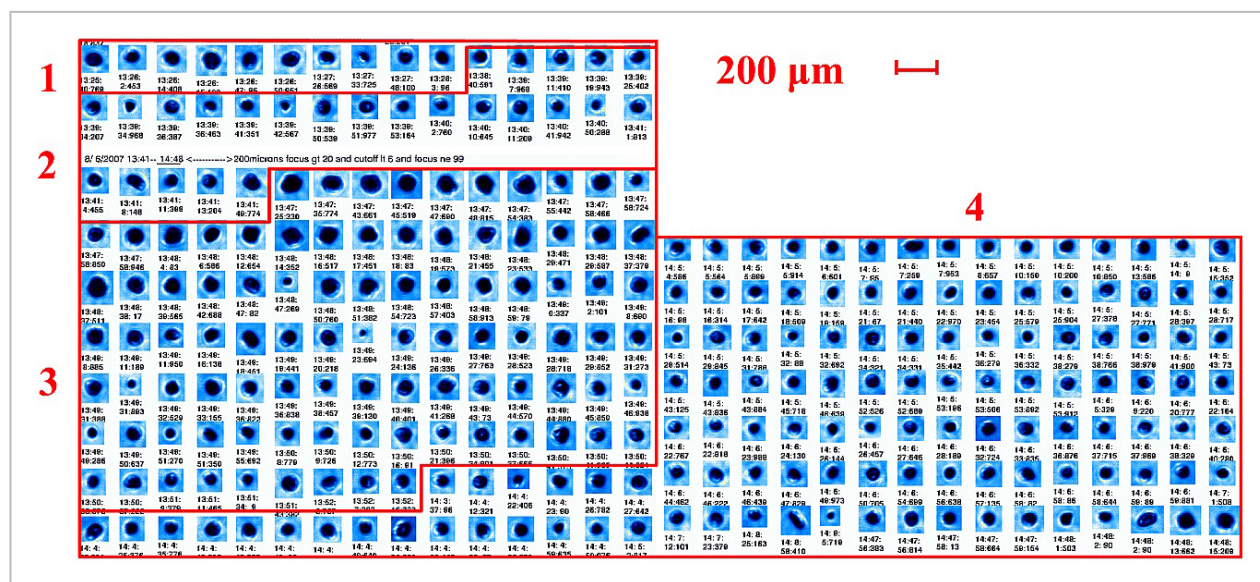


**Figure 4**

[Open in figure viewer](#) | [PowerPoint](#)

All CPI imagery taken during the four SVC passes made by the WB-57F on 6 August 2007.

[22] Because very few particle size distribution measurements have been made in SVC, the shapes of the size distributions are not well characterized by in situ measurements. In [Figure 5](#),

time-averaged size distributions from the 6 August 2007 TC4 SVC are shown along with previous in situ measurements in tropopause SVC. The previous measurements are from near the Marshall Islands in the Western Pacific in December 1973 (ASSP, 1DC, and 1DP data [McFarquhar *et al.*, 2000]), the Indian Ocean during APE-THESEO in 1999 (FSSP-300 [Thomas *et al.*, 2002]), Eastern Pacific during CR-AVE in 2006 [2D-S, Lawson *et al.*, 2008], and tropical West Africa during AMMA in 2006 (FSSP-100 and CIP). Data from imaging probes are in terms of their maximum dimension, whereas those from optical scattering probes assume spherical particles in their sizing. For a consistent comparison, all effective radii are calculated using the mean distributions shown in Figure 5 and assuming spherical particles for IWC and  $A_c$ . Using the more appropriate IWC (with Baker and Lawson IWC( $A_c$ ) relationship) and measured  $A_c$  for 2D-S in this case changes the  $r_e$  by less than 1  $\mu\text{m}$ .

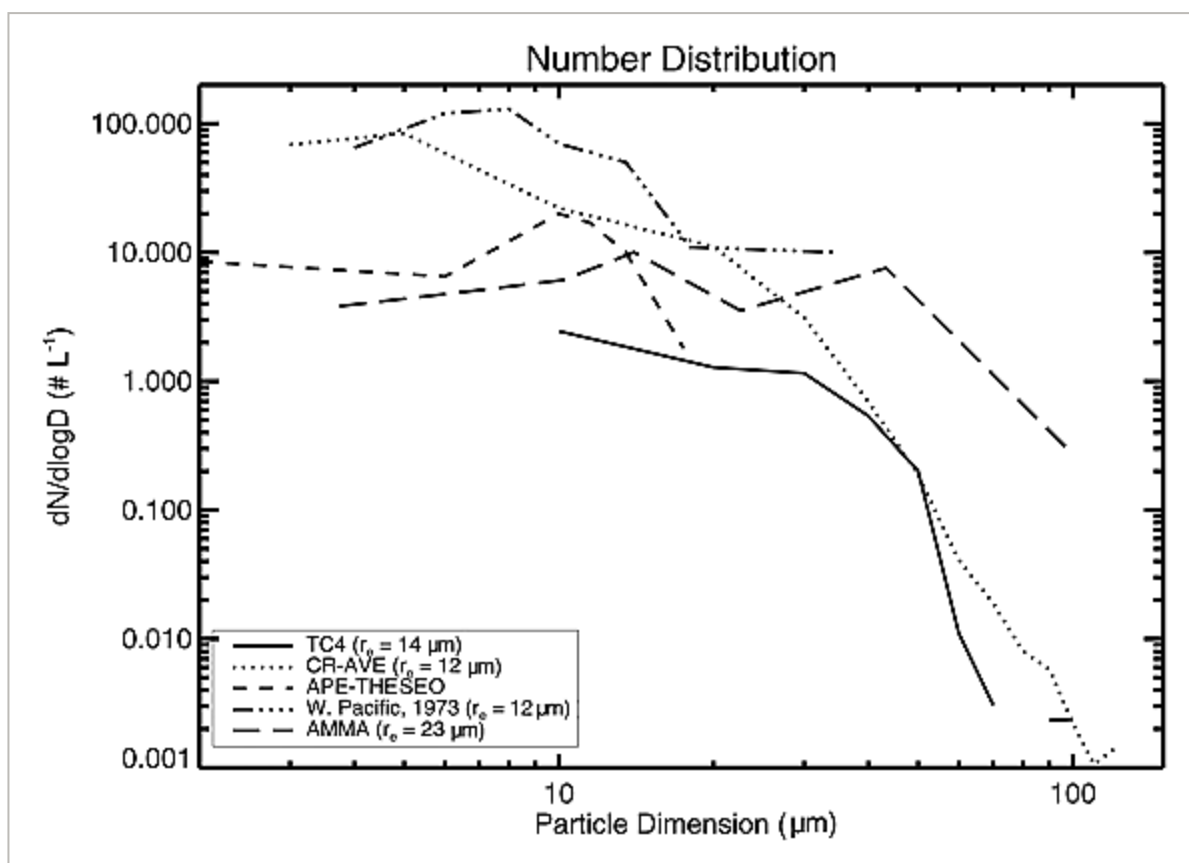


**Figure 5**

[Open in figure viewer](#) | [PowerPoint](#)

Plot of mean size distributions from tropical tropopause subvisible cirrus from various field campaigns.

[23] These distributions are generally similar in shape and have  $r_e$  within a factor of two, which is somewhat surprising given the wide range of geographical locations, seasons, and instruments from which they were taken. The TC4 size distribution appears shifted downwards

compared to the others as a result of the relatively low ice crystal number concentrations present in the SVC layer sampled during TC4.

### 3. SVC Radiative Impact

[24] In this section, a radiative transfer model is used to calculate the perturbation of the tropopause radiative heating rate and impact on top-of-atmosphere radiation due to the presence of the SVC layer. Results presented here are from the Rapid Radiative Transfer Model (RRTM) [[Mlawer and Clough, 1997](#); [Mlawer et al., 1997](#)], although nearly identical values were also found from Libradtran [[Mayer and Kylling, 2005](#)] and the Fu-Liou radiative transfer models [[Fu and Liou, 1993](#)]. RRTM uses a correlated-k method for gaseous absorption, the CKD 2.4 water vapor continuum model [[Clough et al., 1989](#)], and cloud ice parameterizations based on an effective size and water content [[Fu et al., 1998](#); [Fu, 1996](#)]. The key model input parameters relevant to this study are the vertical profiles of atmospheric temperature, ozone, water vapor, and cloud microphysical properties including the ice water path and ice effective radius ( $r_e$ ).

[25] The vertical profiles input into RRTM are shown as dashed lines in [Figure 6](#) (top). Because no single measurement spans the whole altitude range required for input to the model, multiple measurements are combined as described below. For temperature, we use the vertical profile from a Vaisala RS-92 radiosonde launched at 12 UT on 6 August from the Juan Santamaria Airport in Alajuela, Costa Rica. The vertical temperature profile agrees very well with the MMS temperature measurements aboard the WB-57F (within 2 K from the surface to the peak WB-57F altitude, and within 0.4 K from 100–130 hPa), but is used because it extends up to ~10 hPa. Above this level until 1 hPa, the Microwave Limb Sounder (MLS) temperature profile from the nearest Aura overpass (within 500 km) at 7 UT is used. Ozone data are provided by an ECC ozonesonde launched from Alajuela on 7 August 2007 at 6 UT. As with the temperature profile, MLS data are used above ~10 hPa.

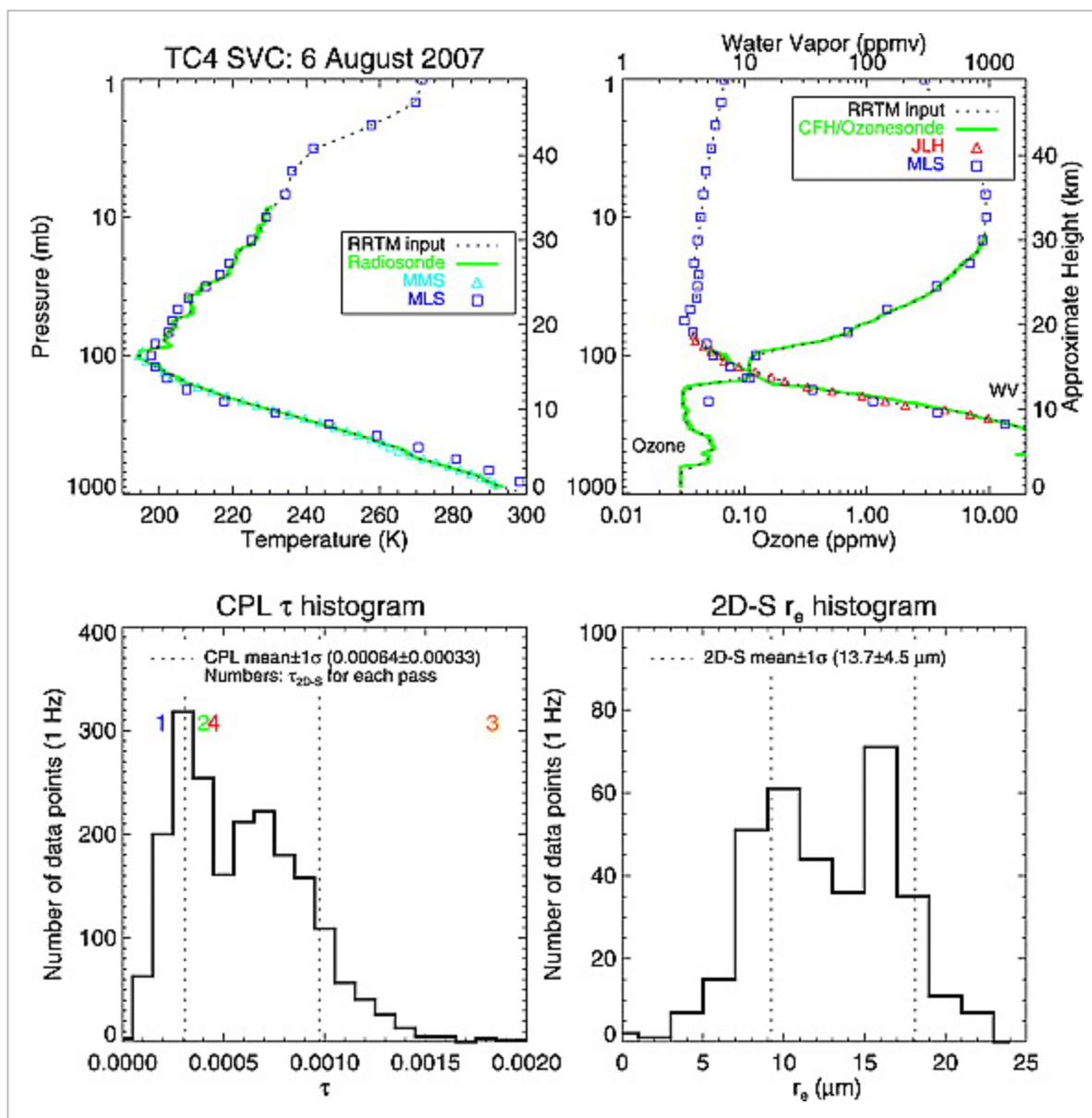


**Figure 6**

[Open in figure viewer](#) | [PowerPoint](#)

Meteorological, trace gas, and SVC microphysical values from the 6 August 2007 TC4 subvisible cirrus and surrounding region used as input for the radiative heating rate calculations. (top) Profiles of temperature, water vapor, and ozone from aircraft, satellite, and balloon measurements. The nominal profile for the radiative heating rate calculation is shown as the dashed line. (bottom left) Values of optical depth from the CPL taken over the SVC layer (12:37–13:25 UT), along with the 2D-S computed optical depth calculated from each of the four passes through the SVC. (bottom right) Values of the 2D-S effective radius from the four SVC passes made by the WB-57F. The lines denote the mean  $\pm 1$  standard deviation of the data.



[26] Water vapor measurements are provided by the JLH from 300 hPa to the peak WB-57F altitude (70 hPa). Below 300 hPa, cryogenic frost-point hygrometer (CFH) [Vömel *et al.*, 2007] data are used from the same payload as the ozonesonde. MLS water vapor data from the nearest overpass are used for altitudes above the WB-57F because CFH data were unavailable on this day above 90 hPa. The JLH data are chosen rather than HW because they are in good agreement with the MLS near the peak WB-57F altitude (within  $\sim 0.5$  ppmv near 100 hPa). As noted previously, the mean difference between HW and JLH is 1.3 ppmv near 100 hPa. This offset is used below for testing the sensitivity of the SVC heating rate results to potential errors associated with the input parameters.

[27] The cloud microphysical input for the cloudy-sky radiative heating rate ( $Z_{\text{cloudy}}$ ) calculations come from the CPL lidar and 2D-S data. The cloud microphysical properties input into the model are IWP (i.e., vertically integrated IWC over the cloud layer) and  $r_e$  for each vertical layer, which are related to the visible optical depth ( $\tau_{\text{vis}}$ ) by

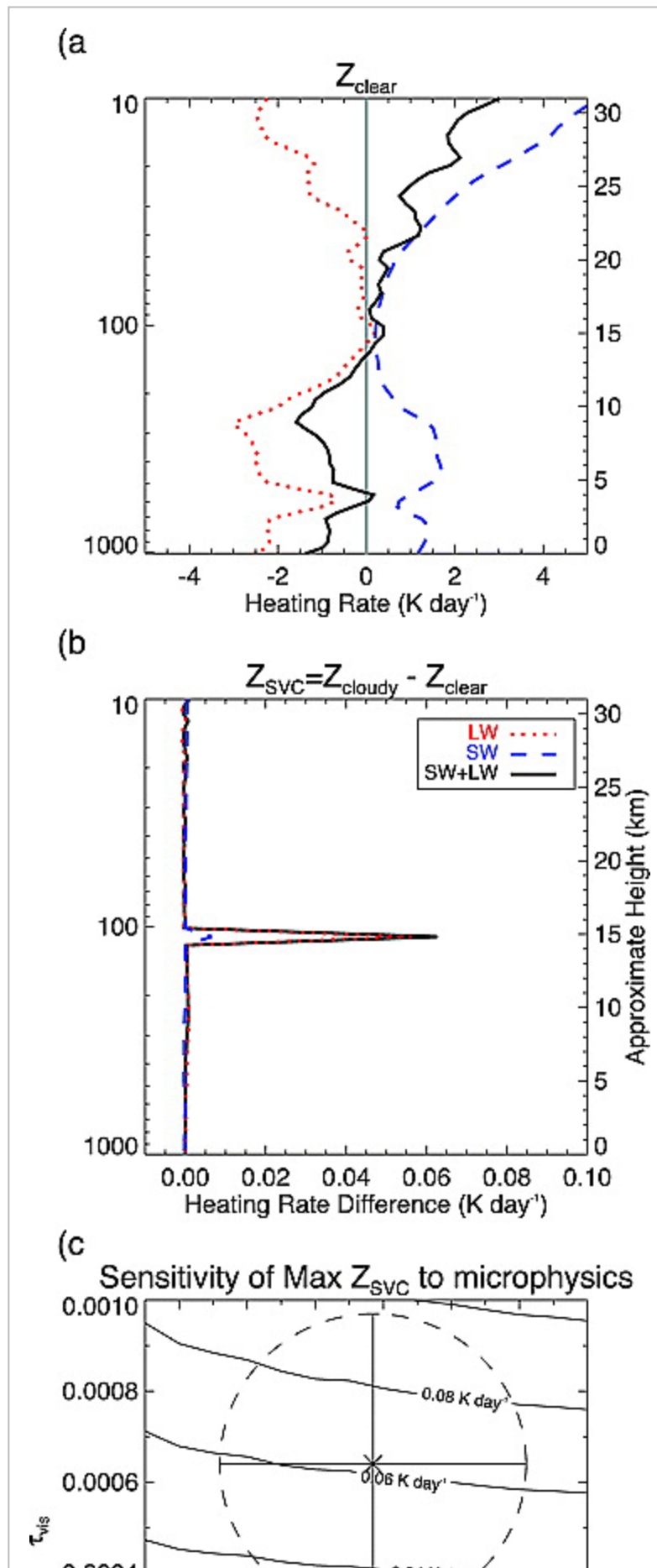
$$\text{IWP} = \frac{2}{3} \rho_{\text{ice}} r_e \tau_{\text{vis}} \quad (1)$$

where IWP is in units  $\text{g m}^{-2}$ ,  $r_e$  is in  $\mu\text{m}$ , and  $\rho_{\text{ice}}$  is the bulk density of ice ( $\sim 0.93 \text{ g cm}^{-3}$ ). For input into the model, we use  $r_e$  from the 2D-S and  $\tau_{\text{vis}}$  from the CPL, and combine these values using (1) to get IWP for input to the model.

[28] The cloud microphysical inputs are shown in [Figure 6](#) (bottom). [Figure 6](#) (bottom left) shows a histogram of the CPL  $\tau_{\text{vis}}$  from the SVC layer (i.e., along AB in [Figure 1](#)), along with the four 2D-S  $\tau_{\text{vis}}$  values calculated from the vertical extinction profiles shown in [Figure 3](#). [Figure 6](#) (bottom right) shows a histogram of the 2D-S  $r_e$  taken during the SVC passes. The vertical lines in [Figure 6](#) (bottom) show the mean  $\pm 1\sigma$  range of the CPL  $\tau_{\text{vis}}$  ( $0.00064 \pm 0.00033$ ) and 2D-S  $r_e$  values ( $13.7 \pm 4.5 \mu\text{m}$ ).

[29] The radiative heating rate results are shown in [Figure 7](#). [Figure 7a](#) shows the clear-sky longwave (LW,  $10\text{--}3250 \text{ cm}^{-1}$ ,  $\sim 3\text{--}1000 \mu\text{m}$ ), shortwave (SW,  $3250\text{--}50,000 \text{ cm}^{-1}$ ,  $\sim 0.2\text{--}3 \mu\text{m}$ ), and net (LW+SW) radiative heating rates. The clear-sky values illustrate that the SVC layer resides in a region of low clear-sky net radiative heating ( $< 1 \text{ K day}^{-1}$ ). In [Figure 7b](#), the LW, SW, and net heating rate differences relative to clear-sky ( $Z_{\text{SVC}} \equiv Z_{\text{cloudy}} - Z_{\text{clear}}$ ) are shown for the mean  $\tau_{\text{vis}}$  and  $r_e$  values given above. This plot illustrates that the SVC layer produces a net positive (warming) radiative heating rate ( $\sim 0.05 \text{ K day}^{-1}$  total), due primarily to LW heating. Despite a small cooling component due to reflection at visible wavelengths,  $Z_{\text{SVC,SW}}$  is slightly positive because the SW wavelength range extends to  $\sim 3 \mu\text{m}$ . These heating rate values are significantly smaller than the values presented by [Bucholtz \*et al.\* \[2010\]](#), [McFarquhar \*et al.\* \[2000\]](#) and [Comstock \*et al.\* \[2002\]](#), who calculated perturbations of  $\sim 0.5\text{--}2 \text{ K day}^{-1}$  for SVC. However, the

primary reason for the difference is that the  $\tau_{\text{vis}}$  considered in the previous studies were significantly higher ( $\sim 0.004\text{--}0.02$ ) than those observed during this TC4 flight.



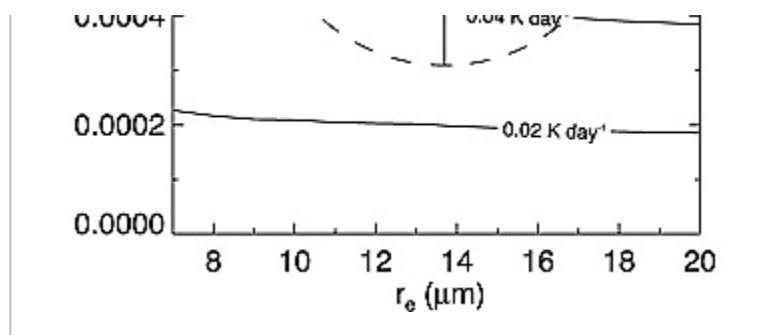


**Figure 7**

[Open in figure viewer](#) | [PowerPoint](#)

Heating rate results and sensitivity to SVC microphysical input. (a) LW, SW, and total (LW+SW) clear-sky heating rates. (b) The heating rate perturbation (relative to clear-sky) due to the presence of SVC ( $Z_{SVC}$ ). (c) Sensitivity of the  $Z_{SVC}$  to the input  $\tau$  and  $r_e$  used for the calculation. The horizontal and vertical error bars denote the  $1\sigma$  range of observed values of  $r_e$  and  $\tau$ , respectively, from [Figure 6](#).

[30] To test the sensitivity of the heating rate results to the input vertical profiles of WV,  $O_3$ , and temperature, tests were performed in which the profile was perturbed from its nominal state. For each variable, a series of tests were run in which either bias or ( $1\sigma$ ) random errors were applied to the profile, with the perturbation values representing approximate measurement uncertainties (1.3 ppmv for WV, 10% for  $O_3$ , and 1 K for temperature).  $Z_{clear}$  can be significantly altered by these perturbations (up to  $0.1 \text{ K day}^{-1}$  near 100 hPa), but the difference in  $Z_{SVC}$  between the perturbed and nominal input cases is negligible ( $<0.002 \text{ K day}^{-1}$ ) because  $Z_{SVC}$  are referenced to the clear-sky value (i.e.,  $Z_{SVC} = Z_{cloudy} - Z_{clear}$ ).

[31] While  $Z_{SVC}$  are not sensitive to realistic uncertainties in WV,  $O_3$ , and temperature, they are somewhat sensitive to the range of  $\tau_{vis}$  and  $r_e$  values illustrated in [Figure 7c](#). [Figure 7c](#) shows a contour plot of the heating rate calculated for  $\tau_{vis}$  in the range  $10^{-4}$ – $10^{-3}$ , and  $r_e$  in the range 7–20  $\mu\text{m}$ . The horizontal and vertical bars in [Figure 7c](#) represent the mean  $\pm 1\sigma$  of the CPL  $\tau_{vis}$  and 2D-S  $r_e$  values shown in [Figure 6](#). As can be seen in [Figure 7c](#),  $Z_{SVC}$  are more sensitive to  $\tau_{vis}$  than to  $r_e$  over the  $1\sigma$  range of values measured by the CPL and 2D-S. For example, the range of  $Z_{SVC}$  corresponding to only varying  $r_e$  (by  $\pm 1\sigma$ ) is  $0.058$ – $0.066 \text{ K day}^{-1}$ , whereas the range corresponding to varying  $\tau_{vis}$  is  $0.031$ – $0.095 \text{ K day}^{-1}$ . The range of  $Z_{SVC}$  encompassed by the  $1\sigma$  ellipse in [Figure 7c](#) is the same as for  $\tau_{vis}$ .

[32] Finally, the net TOA cloud radiative effect (CRE), defined here as the clear minus cloudy sky difference in total (SW+LW) upward flux, is calculated. The CRE from the nominal SVC case is  $0.013 \text{ W m}^{-2}$ , with a  $0.092 \text{ W m}^{-2}$  LW effect that is mostly compensated for by a  $-0.079 \text{ W m}^{-2}$  SW effect. Considering the range of  $\tau_{vis}$  and  $r_e$  shown in [Figures 6](#) and [7](#), the range of CRE is



0.001–0.03 W m<sup>-2</sup>. These results are much smaller than previous estimates for SVC [[Comstock et al., 2002](#); [McFarquhar et al., 2000](#)], which were ~1 W m<sup>-2</sup>. However, our results are merely reflective of the thinness of this particular SVC, and should not be construed as being in disagreement with previous work. The RRTM model gives similar values for cloud radiative effects if one inputs optical depths similar to these previous studies.

## 4. Lidar-Based SVC Observations During TC4

[33] In this section, aircraft and satellite-based lidar observations of tropopause SVC are analyzed in order to place into context the extremely thin SVC layer observed during the 6 August 2007 TC4 flight. One of the main goals of this effort is to understand whether properties of the 6 August cloud are anomalous for this geographic region and season based on CPL observations during the other TC4 flights. Also, we address the issue of how the TC4 CPL data compares to previous aircraft lidar data, and how they compare to satellite-based lidar observations from the Cloud-Aerosol Lidar and Infrared Pathfinder Satellite Observation (CALIPSO) satellite in the TC4 region (identified in [Figure 1](#)).

[34] The ER-2 flew 11 flights based out of San Jose, Costa Rica between July 17 and August 8, 2007. During these flights, the CPL obtained 51 hours of data in the tropics (see [Figure 1](#)), corresponding to approximately 37,000 km of distance. The CPL data used here have been analyzed using a layer detection algorithm that detects up to 10 layers of aerosol and/or cloud (D. Hlavka et al., Vertical cloud climatology during TC4 derived from high-altitude aircraft merged lidar and radar profiles, submitted to *Journal of Geophysical Research*, 2010). The statistics presented here are for cases where the cloud base of the uppermost layer detected by the CPL or CALIPSO is above 15 km (i.e., the same definition used by [McFarquhar et al. \[2000\]](#)). Also, the data used are from the CALIPSO comparison region shown in [Figure 1](#) (90–78 W, 4–14 N), as this region was more evenly-sampled by the ER-2 during TC4, and makes for a more valid comparison with CALIPSO.

[35] Many of the TC4 ER-2 flights were coordinated with the DC-8 as it sampled clouds lower in the atmosphere, so in general the ER-2 CPL data in the mid-troposphere are biased towards cloudy conditions at DC-8 altitudes around 10–12 km (Hlavka et al., submitted manuscript, 2010). However, despite the bias towards cloudy conditions at lower levels, it is unlikely that the CPL data at the tropopause level (~17 km) are biased in terms of their sampling of SVC vs. SVC-free air. One reason for this lack of bias is that SVC, as defined here with cloud base height >15 km, are more likely formed by local cooling rather than direct detrainment from deep convection (mean convective cloud-top height from CPL was 12.4 km during TC4 (Hlavka et al., submitted manuscript, 2010)). Also, the waves that provide the local cooling for in situ SVC formation are not necessarily linked to local convection [[Boehm and Verlinde, 2000](#)], SVC have a long lifetime (~days), and can be advected over large distances [[Jensen et al., 1996a, 1996b](#); [Luo](#)

[et al., 2003a](#); [Peter et al., 2003](#); [Pfister et al., 2001](#)]. Taken together, these aspects of SVC suggest that the CPL SVC occurrence statistics and microphysical properties should be reasonably representative of conditions in the Eastern Pacific region for this time of year, with the main caveat being the limited amount of data collected by the ER-2.

[36] [Figure 8](#) shows 2D histograms of the relationships between height and physical properties for clouds with base heights >15 km observed by CPL during TC4, and by CALIPSO during July–August 2007 within the box shown in [Figure 1](#). In general, both  $\tau$  and cloud thickness decrease with increasing cloud height. However, because a decrease in thickness would lead to a decrease in  $\tau$  for a given  $\beta$ , it is possible that merely a thinning of the cloud layers with increasing height could explain the trend in  $\tau$ . But as shown in [Figure 8](#), the cloud-layer mean  $\beta$  (defined as  $\tau/\Delta z$ ) also decreases with height. Thus, the decrease with height of  $\tau$  is due to both decreases in cloud thickness as well as decreases in extinction. This is not a surprising result due to the lack of available water for condensation at these temperatures, and has been qualitatively seen in other studies (e.g., in cirrus IWC [[Schiller et al., 2008](#)]).

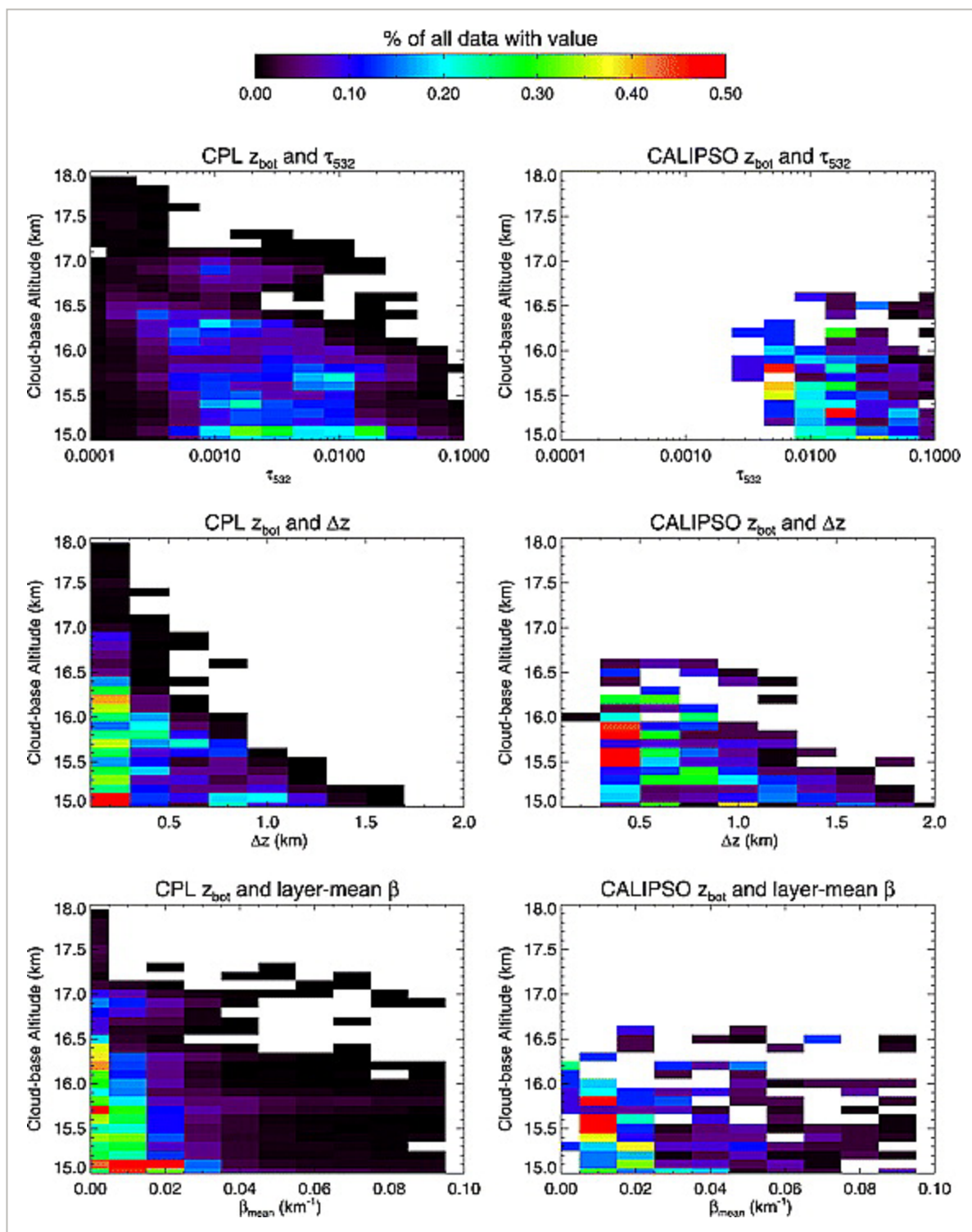


**Figure 8**

[Open in figure viewer](#) | [PowerPoint](#)

2D histograms of SVC (with  $z_{\text{bot}} > 15$  km) properties observed by the CPL and CALIPSO during TC4: (left) CPL data from TC4 and (right) CALIPSO data over the comparison region shown in Figure 1.

[37] Histograms of SVC relative frequency (number of SVC observations with a given  $\tau$  divided by the total number of SVC observations) and occurrence frequency (number of SVC observations with a given  $\tau$  divided by the total number of observations) are shown in [Figure 9](#). [Figure 9a](#) shows the relative frequency of SVC observations (relative to the total number of SVC observations during TC4) for the 6 August flight, other TC4 flights, and all TC4 flights. As can be seen from [Figure 9](#), most of the SVC observations from the 6 August flight had  $\tau < 0.002$ , but many cloud layers with similar optical depth were measured during other flights. This indicates that the thinness of the SVC layer observed on 6 August was not an outlier among the overall distribution of CPL SVC data.

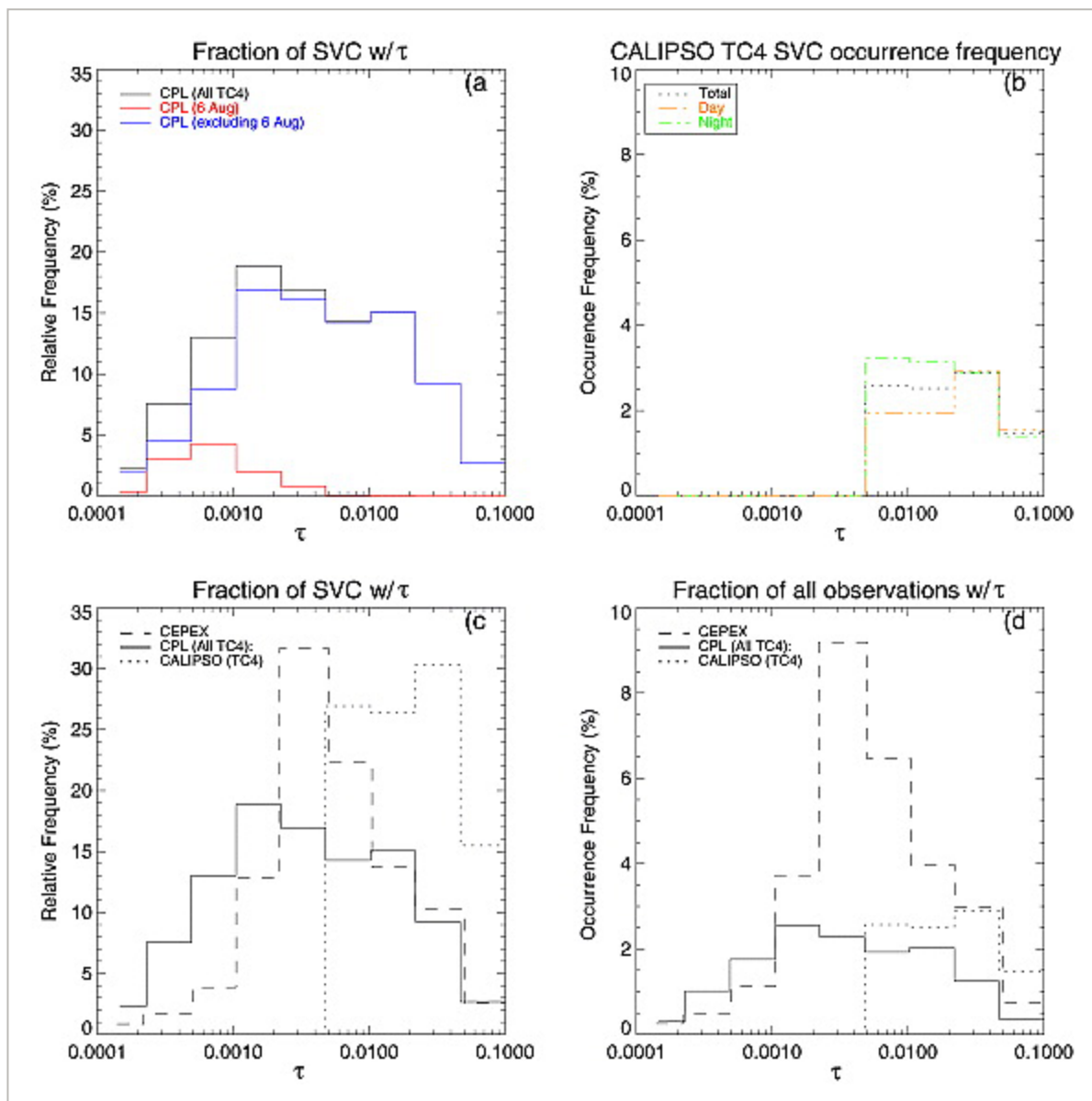


**Figure 9**

[Open in figure viewer](#) | [PowerPoint](#)



SVC (with  $z_{\text{bot}} > 15$  km) frequency histograms. Relative frequency refers to the number of SVC observations that occur within a given  $\tau$  bin relative to the total number of SVC observations. Occurrence frequency refers to the number of SVC that occur within a given  $\tau$  bin, relative to the total number of observations (i.e., both SVC and clear-sky). (a) The relative frequency of SVC during TC4 (numbers are relative to the total number of CPL SVC observations during all flights). The 6 August case is shown separately to highlight its contribution to the overall distribution. (b) Occurrence frequency of SVC from CALIPSO over the TC4 geographic region defined in [Figure 1](#) during July–August, 2007. Data broken down by day vs. night show slightly larger occurrence frequencies at night, probably due to enhanced sensitivity by the lidar. (c) Relative frequency of SVC seen by aircraft lidar during CEPEX [[McFarquhar et al., 2000](#), Figure 9], and by aircraft (CPL) and satellite (CALIPSO) lidar during TC4. (d) Same as (c), but for SVC occurrence frequency. Note that CEPEX occurrence frequency data have been scaled to match the total value of 29% provided by [McFarquhar et al. \[2000\]](#).

[38] Also shown in [Figure 9](#) are CALIPSO data taken in July–August 2007 in the geographic region marked in [Figure 1](#). [Figure 9b](#) shows the diurnal variation of SVC occurrence frequency as a function of  $\tau_{\text{vis}}$  from CALIPSO, using the retrieval described in [Yang et al. \[2010\]](#). CALIPSO sees a slight increase in the occurrence of the thinnest SVC at night, probably due to its better nighttime sensitivity. However, there is no increase in the minimum  $\tau$  of SVC detected by CALIPSO at night in this region.

[39] [Figure 9c](#) shows a histogram of SVC relative occurrence frequency from CEPEX and TC4. Overall, the CEPEX distribution is quite similar to the TC4 distribution, but there are significant differences between the CPL and CALIPSO distributions in [Figure 9c](#). CALIPSO does not observe any clouds with  $\tau < 0.006$ , whereas a significant fraction of both TC4 CPL SVC data and CEPEX data have  $\tau < 0.006$  (63% for all TC4 flights, 59% for flights other than 6 August, and ~50% for CEPEX).

[40] The differences among the distributions in [Figure 9c](#) are also presented in terms of the SVC occurrence frequency in [Figure 9d](#). For SVC with  $z_{\text{bot}} > 15$  km and within the TC4 region defined above, occurrence frequencies from CPL were 38% for the 6 August flight, 13% for all other flights, and 14% for the whole TC4 mission. For CALIPSO, the occurrence frequency (day+night combined) is 10% for the TC4 region. Occurrence frequency values in the TC4 geographic region for July–August 2006 and 2008 (not shown) are similar to that for 2007. It is interesting to note that the overall occurrence frequencies are fairly similar between CPL and CALIPSO (14% vs. 10%, respectively), even though CALIPSO does not observe any clouds with  $\tau < 0.006$  and observes more thicker clouds (with  $\tau > 0.006$ ) than CPL. It is possible that some of the

difference is caused by the limited and potentially biased spatial sampling of the region by the ER-2.

[41] Both the CPL and CALIPSO SVC occurrence frequency values during TC4 are significantly lower than the CEPEX value of 29% provided by [McFarquhar et al. \[2000\]](#). Differences between the TC4 and CEPEX SVC frequencies are not necessarily surprising given the seasonal and geographical differences previously indicated by satellite measurements [[Winker and Trepte, 1998](#); [Yang et al., 2010](#)]. The differences could be due to the greater incidence of convection that is likely present during the Central Pacific winter (CEPEX) versus Eastern Pacific summer (TC4).

[42] It is worth noting that several other studies have obtained estimates of ~50% occurrence frequency for optically thin tropical cirrus [[Nee et al., 1998](#); [Prabhakara et al., 1988](#); [Wang et al., 1994](#)], but these values are not directly comparable to the TC4 CPL data presented here because the studies did not specifically consider SVC near the tropopause. These estimates are actually quite similar to the upper tropospheric cloud occurrence frequency from the CPL during TC4, which was 42% (Hlavka et al., submitted manuscript, 2010).

[43] The mean(median)  $\pm$  one standard deviation ( $1\sigma$ ) of CPL  $\tau$  values for clouds with  $z_{\text{bot}} > 15$  km is  $0.043(0.0030) \pm 0.32$ , and the CALIPSO values are  $0.035(0.020) \pm 0.056$ . Excluding clouds with  $\tau > 0.1$ , which was effectively the value chosen by [McFarquhar et al. \[2000\]](#) in their analysis of tropopause cirrus, the CPL and CALIPSO values are  $0.0082(0.0029) \pm 0.013$  and  $0.025(0.019) \pm 0.021$ , compared to the CEPEX value of  $0.0045 \pm 0.014$  (mean  $\pm 1\sigma$ ). As evidenced by the differences between the mean and median values above and the histograms in [Figure 9](#), the distributions of SVC are highly skewed, so caution should be taken when interpreting the radiative implications of these results.

## 5. Conclusions

[44] On the 6 August 2007 flight of the TC4 field campaign, the CPL aboard the NASA ER-2 aircraft indicated an extensive and extremely optically thin ( $\tau \sim 0.0006$ ) layer of laminar subvisible cirrus near the tropopause (~400 km long and ~500 m thick). Using this information, the WB-57F aircraft was directed to porpoise through the layer, making in situ measurements along the same track flown by the ER-2 approximately an hour earlier. From these maneuvers, vertical profiles of temperature, water vapor, and cloud microphysical properties were made from aboard the WB-57F. These data add to the relatively sparse set of in situ measurements collected in tropical tropopause SVC, and were shown to be qualitatively similar to previous studies. The measurements support previous observations indicating that SVC exist within a relatively narrow saturated layer just below the tropical cold-point tropopause.

[45] In this paper, we calculated the radiative heating rates and cloud radiative effect for the SVC layer sampled on the 6 August 2007 TC4 flight. Using the range of optical depths ( $\sim 10^{-4}$ – $10^{-3}$ ) and effective sizes ( $\sim 9$ – $18 \mu\text{m}$ ) provided by the in situ and remote sensing measurements, we found heating rates in the range  $0.03$ – $0.1 \text{ K day}^{-1}$  for this layer, and cloud radiative forcing values  $\sim 0.001$ – $0.03 \text{ W m}^{-2}$ . These values are significantly lower than previous estimates of  $\sim 0.5$ – $2 \text{ K day}^{-1}$  and  $\sim 1 \text{ W m}^{-2}$ , due to the relative thinness of the SVC reported here.

[46] Given their location just below the cold-point tropopause and positive net radiative heating, it has been previously suggested that tropopause SVC serve as the final step in the dehydration of air as it enters the stratosphere [[Luo et al., 2003a](#)]. If irreversible dehydration was occurring in the SVC sampled by the WB-57F during TC4 as it ascended through the cold-point into the warmer stratosphere, then an upper-bound estimate of this final dehydration is given by the IWC of the cloud, which is at most  $0.5 \text{ ppmv}$ .

[47] However, while it is possible that irreversible dehydration of air was occurring in this cloud, the presence of SVC as a climatological feature could also act to increase the entry value of stratospheric water vapor through their warming influence on tropical tropopause temperatures [[Rosenfield et al., 1998](#)]. [Rosenfield et al. \[1998\]](#) showed with a 2D model that including tropopause SVC with (zonally-averaged) heating rates  $\sim 0.1$ – $0.2 \text{ K day}^{-1}$  led to a  $1 \text{ ppmv}$  increase in stratospheric water vapor. Although the heating rates presented here are also  $\sim 0.1 \text{ K day}^{-1}$ , the global and seasonal distributions of these clouds would need to be known in order to even begin to make a comparison to the model results. The data presented here are insufficient to estimate the net effect of tropopause SVC on the stratospheric water budget, but the magnitude of the IWC and heating rate values support the idea that even the thinnest of these ultrathin clouds play a non-negligible role in determining the entry value of stratospheric water vapor.

[48] Finally, the TC4 in situ and CPL SVC data highlight the fact that estimates of the occurrence frequency of thin tropopause cirrus from satellite-borne instruments such as CALIPSO are likely to miss a significant fraction of subvisible cirrus clouds. As an example, in the tropics ( $30 \text{ S}$ – $30 \text{ N}$ ),  $\sim 20\%$  ( $\sim 0.008\%$ ) of tropopause clouds (with  $z_{\text{bottom}} > 15 \text{ km}$ ) detected by CALIPSO have  $\tau < 0.01$  ( $\tau < 0.001$ ), whereas in the TC4 CPL data set the number is  $73\%$  ( $24\%$ ). Even excluding the anomalously thin SVC from the 6 August flight, the percentage of CPL data with  $\tau < 0.01$  ( $\tau < 0.001$ ) is  $70\%$  ( $18\%$ ), and for CEPEX the value is  $\sim 70\%$  ( $\sim 6\%$ ). As an illustration, taking the most conservative aircraft-based estimate for the fraction of SVC with  $\tau < 0.01$  ( $70\%$ ), this would imply that CALIPSO would be missing  $\sim 2/3$  of these clouds.

[49] Ideally, extensive and truly random sampling of tropopause SVC by airborne lidars is needed in order to facilitate a detailed intercomparison of cirrus statistics with CALIPSO and help quantify the fraction of ultrathin clouds missed by CALIPSO. At this point, it is not possible

to know accurately how widespread clouds that fall below the detection limit of CALIPSO are, and further study is needed to address whether or not they could contribute significantly to the radiation and water vapor budget of the TTL region.

## Acknowledgments

[50] The authors would like to acknowledge the efforts of the TC4 mission planners and instrument investigators, as well as the pilots and staff of the WB-57F and ER-2 aircraft. The authors would also like to acknowledge the CPL instrument team, led by P.I. Matt McGill. S.M.D. would like to thank Karl Froyd, Bob Portmann, and Anthony Bucholtz for helpful discussions and reviews. S.M.D. acknowledges support from Linnea Avallone under NASA Radiation Sciences Program grant NNX07AL20G, and the NOAA atmospheric composition and climate program.

## References



Baker, B., and Lawson, R. P. ( 2006), Improvement in determination of ice water content from two-dimensional particle imagery. Part I: Image-to-mass relationships, *J. Appl. Meteorol. Climatol.*, **45**( 9), 1282– 1290, doi:[10.1175/JAM2398.1](https://doi.org/10.1175/JAM2398.1) .

[Crossref](#) | [ADS](#) | [Web of Science®](#) | [Google Scholar](#)

Boehm, M. T., and Verlinde, J. ( 2000), Stratospheric influence on upper tropospheric tropical cirrus, *Geophys. Res. Lett.*, **27**( 19), 3209– 3212, doi:[10.1029/2000GL011678](https://doi.org/10.1029/2000GL011678) .

[Wiley Online Library](#) | [ADS](#) | [Web of Science®](#) | [Google Scholar](#)

Bucholtz, A., Hlavka, D. L., McGill, M., Schmidt, K. S., Pilewskie, P., Davis, S. M., Reid, E. A., and Walker, A. L. ( 2010), Directly measured heating rates of a tropical subvisible cirrus cloud, *J. Geophys. Res.*, **115**, D00J09, doi:[10.1029/2009JD013128](https://doi.org/10.1029/2009JD013128) .

[Wiley Online Library](#) | [ADS](#) | [PubMed](#) | [Web of Science®](#) | [Google Scholar](#)

Clough, S. A., et al. ( 1989), Line shape and the water vapor continuum, *Atmos. Res.*, **23**( 3–4), 229– 241, doi:[10.1016/0169-8095\(89\)90020-3](https://doi.org/10.1016/0169-8095(89)90020-3) .

[Crossref](#) | [ADS](#) | [Google Scholar](#)

Comstock, J. M., et al. ( 2002), Ground-based lidar and radar remote sensing of tropical cirrus clouds at Nauru Island: Cloud statistics and radiative impacts, *J. Geophys. Res.*, **107**( D23), 4714, doi:[10.1029/2002JD002203](https://doi.org/10.1029/2002JD002203) .

[Wiley Online Library](#) | [ADS](#) | [Web of Science®](#) | [Google Scholar](#)

Corti, T., et al. ( 2006), The impact of cirrus clouds on tropical troposphere-to-stratosphere transport, *Atmos. Chem. Phys.*, **6**, 2539– 2547, doi:[10.5194/acp-6-2539-2006](https://doi.org/10.5194/acp-6-2539-2006) .



[Crossref](#) | [CAS](#) | [ADS](#) | [Web of Science®](#) | [Google Scholar](#)

---

Dvortsov, V. L., and Solomon, S. ( 2001), Response of the stratospheric temperatures and ozone to past and future increases in stratospheric humidity, *J. Geophys. Res.*, **106**( D7), 7505– 7514, doi:[10.1029/2000JD900637](https://doi.org/10.1029/2000JD900637) .

[Wiley Online Library](#) | [CAS](#) | [ADS](#) | [Web of Science®](#) | [Google Scholar](#)

---

Forster, P. M. D., and Shine, K. P. ( 2002), Assessing the climate impact of trends in stratospheric water vapor, *Geophys. Res. Lett.*, **29**( 6), 1086, doi:[10.1029/2001GL013909](https://doi.org/10.1029/2001GL013909) .

[Wiley Online Library](#) | [ADS](#) | [Web of Science®](#) | [Google Scholar](#)

---

Fu, Q. A. ( 1996), An accurate parameterization of the solar radiative properties of cirrus clouds for climate models, *J. Clim.*, **9**( 9), 2058– 2082, doi:[10.1175/1520-0442\(1996\)009<2058:AAPOTS>2.0.CO;2](https://doi.org/10.1175/1520-0442(1996)009<2058:AAPOTS>2.0.CO;2).

[Crossref](#) | [ADS](#) | [Web of Science®](#) | [Google Scholar](#)

---

Fu, Q., and Liou, K. N. ( 1993), Parameterization of the radiative properties of cirrus clouds, *J. Atmos. Sci.*, **50**( 13), 2008– 2025, doi:[10.1175/1520-0469\(1993\)050<2008:POTRPO>2.0.CO;2](https://doi.org/10.1175/1520-0469(1993)050<2008:POTRPO>2.0.CO;2) .

[Crossref](#) | [ADS](#) | [Web of Science®](#) | [Google Scholar](#)

---

Fu, Q., et al. ( 1998), An accurate parameterization of the infrared radiative properties of cirrus clouds for climate models, *J. Clim.*, **11**( 9), 2223– 2237, doi:[10.1175/1520-0442\(1998\)011<2223:AAPOTI>2.0.CO;2](https://doi.org/10.1175/1520-0442(1998)011<2223:AAPOTI>2.0.CO;2) .

[Crossref](#) | [ADS](#) | [Web of Science®](#) | [Google Scholar](#)

---

Gao, R. S., et al. ( 2004), Evidence that nitric acid increases relative humidity in low-temperature cirrus clouds, *Science*, **303**( 5657), 516– 520, doi:[10.1126/science.1091255](https://doi.org/10.1126/science.1091255) .

[Crossref](#) | [CAS](#) | [ADS](#) | [PubMed](#) | [Web of Science®](#) | [Google Scholar](#)

---

Gensch, I. V., et al. ( 2008), Supersaturations, microphysics and nitric acid partitioning in a cold cirrus cloud observed during CR-AVE 2006: An observation-modelling intercomparison study, *Environ. Res. Lett.*, **3**( 3), 035003, doi:[10.1088/1748-9326/3/3/035003](https://doi.org/10.1088/1748-9326/3/3/035003) .

[Crossref](#) | [CAS](#) | [ADS](#) | [PubMed](#) | [Web of Science®](#) | [Google Scholar](#)

---

Haladay, T., and Stephens, G. ( 2009), Characteristics of tropical thin cirrus clouds deduced from joint CloudSat and CALIPSO observations, *J. Geophys. Res.*, **114**, D00A25, doi:[10.1029/2008JD010675](https://doi.org/10.1029/2008JD010675) .

[Wiley Online Library](#) | [ADS](#) | [PubMed](#) | [Web of Science®](#) | [Google Scholar](#)

---

Heymsfield, A. J. ( 1986), Ice particles observed in a cirriform cloud at  $-83^{\circ}\text{C}$  and implications for polar stratospheric clouds, *J. Atmos. Sci.*, **43**( 8), 851– 855, doi:[10.1175/1520-0469\(1986\)043<0851:IPOIAC>2.0.CO;2](https://doi.org/10.1175/1520-0469(1986)043<0851:IPOIAC>2.0.CO;2) .

[Crossref](#) | [ADS](#) | [Web of Science®](#) | [Google Scholar](#)

---

Heymsfield, A. J., and Jahnsen, L. J. ( 1974), Microstructure of tropopause cirrus layers, paper presented at Sixth Conference on Aerospace and Aeronautical Meteorology, Am. Meteorol. Soc. El Paso, Tex.

[Google Scholar](#)

---

Hints, E. J., et al. ( 1999), On the accuracy of in situ water vapor measurements in the troposphere and lower stratosphere with the Harvard Lyman-alpha hygrometer, *J. Geophys. Res.*, **104**( D7), 8183–8189, doi:[10.1029/1998JD100110](https://doi.org/10.1029/1998JD100110) .

[Wiley Online Library](#) | [CAS](#) | [ADS](#) | [Web of Science®](#) | [Google Scholar](#)

---

Jensen, E. J., et al. ( 1996a), Dehydration of the upper troposphere and lower stratosphere by subvisible cirrus clouds near the tropical tropopause, *Geophys. Res. Lett.*, **23**( 8), 825– 828, doi:[10.1029/96GL00722](https://doi.org/10.1029/96GL00722) .

[Wiley Online Library](#) | [ADS](#) | [Web of Science®](#) | [Google Scholar](#)

---

Jensen, E. J., et al. ( 1996b), On the formation and persistence of subvisible cirrus clouds near the tropical tropopause, *J. Geophys. Res.*, **101**( D16), 21,361– 21,375, doi:[10.1029/95JD03575](https://doi.org/10.1029/95JD03575) .

[Wiley Online Library](#) | [ADS](#) | [Web of Science®](#) | [Google Scholar](#)

---

Jensen, E. J., et al. ( 2008), Formation of large ( $\approx 100 \mu\text{m}$ ) ice crystals near the tropical tropopause, *Atmos. Chem. Phys.*, **8**( 6), 1621– 1633, doi:[10.5194/acp-8-1621-2008](https://doi.org/10.5194/acp-8-1621-2008) .

[Crossref](#) | [CAS](#) | [ADS](#) | [Web of Science®](#) | [Google Scholar](#)

---

Jensen, E. J., et al. ( 2009), On the importance of small ice crystals in tropical anvil cirrus, *Atmos. Chem. Phys.*, **9**( 15), 5519– 5537, doi:[10.5194/acp-9-5519-2009](https://doi.org/10.5194/acp-9-5519-2009) .

[Crossref](#) | [CAS](#) | [ADS](#) | [Web of Science®](#) | [Google Scholar](#)

---

Jensen, E. J., et al. ( 2010), Ice nucleation and cloud microphysical properties in tropical tropopause layer cirrus, *Atmos. Chem. Phys.*, **10**( 3), 1369– 1384, doi:[10.5194/acp-10-1369-2010](https://doi.org/10.5194/acp-10-1369-2010) .

[Crossref](#) | [CAS](#) | [ADS](#) | [Web of Science®](#) | [Google Scholar](#)

---

Kley, D., et al. ( 2000), SPARC Assessment of Upper Tropospheric and Stratospheric Water Vapour, *WCRP-113*, World Clim. Res. Programme, Geneva, Switzerland. (Available at [http://www.atmosp.physics.utoronto.ca/SPARC/WAVASFINAL\\_000206/WWW\\_wavas/Cover.html](http://www.atmosp.physics.utoronto.ca/SPARC/WAVASFINAL_000206/WWW_wavas/Cover.html) ).

[Google Scholar](#)

---

Korolev, A. ( 2007), Reconstruction of the sizes of spherical particles from their shadow images. Part I: Theoretical considerations, *J. Atmos. Oceanic Technol.*, **24**( 3), 376– 389, doi:[10.1175/JTECH1980.1](https://doi.org/10.1175/JTECH1980.1) .

[Crossref](#) | [ADS](#) | [Web of Science®](#) | [Google Scholar](#)

---

Krämer, M., et al. ( 2009), Ice supersaturations and cirrus cloud crystal numbers, *Atmos. Chem. Phys.*, **9**( 11), 3505– 3522, doi:[10.5194/acp-9-3505-2009](https://doi.org/10.5194/acp-9-3505-2009) .

[Crossref](#) | [ADS](#) | [Web of Science®](#) | [Google Scholar](#)

---

---

Lawson, R. P., Baker, B. A., Schmitt, C. G., and Jensen, T. L. ( 2001), An overview of microphysical properties of Arctic clouds observed in May and July 1998 during FIRE ACE, *J. Geophys. Res.*, **106**, 14,989– 15,014, doi:[10.1029/2000JD900789](https://doi.org/10.1029/2000JD900789) .

[Wiley Online Library](#) | [ADS](#) | [Web of Science®](#) | [Google Scholar](#)

---

Lawson, R. P., et al. ( 2006), The 2D-S (Stereo) probe: Design and preliminary tests of a new airborne, high-speed, high-resolution particle Imaging probe, *J. Atmos. Oceanic Technol.*, **23**( 11), 1462– 1477, doi:[10.1175/JTECH1927.1](https://doi.org/10.1175/JTECH1927.1) .

[Crossref](#) | [ADS](#) | [Web of Science®](#) | [Google Scholar](#)

---

Lawson, R. P., et al. ( 2008), Aircraft measurements of microphysical properties of subvisible cirrus in the tropical tropopause layer, *Atmos. Chem. Phys.*, **8**( 6), 1609– 1620, doi:[10.5194/acp-8-1609-2008](https://doi.org/10.5194/acp-8-1609-2008) .

[Crossref](#) | [CAS](#) | [ADS](#) | [Web of Science®](#) | [Google Scholar](#)

---

Luo, B. P., et al. ( 2003a), Dehydration potential of ultrathin clouds at the tropical tropopause, *Geophys. Res. Lett.*, **30**( 11), 1557, doi:[10.1029/2002GL016737](https://doi.org/10.1029/2002GL016737) .

[Wiley Online Library](#) | [ADS](#) | [Web of Science®](#) | [Google Scholar](#)

---

Luo, B. P., et al. ( 2003b), Ultrathin Tropical Tropopause Clouds (UTTCs): II. Stabilization mechanisms, *Atmos. Chem. Phys.*, **3**, 1093– 1100, doi:[10.5194/acp-3-1093-2003](https://doi.org/10.5194/acp-3-1093-2003) .

[Crossref](#) | [CAS](#) | [ADS](#) | [Web of Science®](#) | [Google Scholar](#)

---

May, R. D. ( 1998), Open-path, near-infrared tunable diode laser spectrometer for atmospheric measurements of H<sub>2</sub>O, *J. Geophys. Res.*, **103**( D15), 19,161– 19,172, doi:[10.1029/98JD01678](https://doi.org/10.1029/98JD01678) .

[Wiley Online Library](#) | [CAS](#) | [ADS](#) | [Web of Science®](#) | [Google Scholar](#)

---

Mayer, B., and Kylling, A. ( 2005), Technical note: The libRadtran software package for radiative transfer calculations—Description and examples of use, *Atmos. Chem. Phys.*, **5**, 1855– 1877, doi:[10.5194/acp-5-1855-2005](https://doi.org/10.5194/acp-5-1855-2005) .

[Crossref](#) | [CAS](#) | [ADS](#) | [Web of Science®](#) | [Google Scholar](#)

---

McFarquhar, G. M., et al. ( 2000), Thin and subvisual tropopause tropical cirrus: Observations and radiative impacts, *J. Atmos. Sci.*, **57**( 12), 1841– 1853, doi:[10.1175/1520-0469\(2000\)057<1841:TASTTC>2.0.CO;2](https://doi.org/10.1175/1520-0469(2000)057<1841:TASTTC>2.0.CO;2) .

[Crossref](#) | [ADS](#) | [Web of Science®](#) | [Google Scholar](#)

---

McGill, M., et al. ( 2002), Cloud Physics Lidar: Instrument description and initial measurement results, *Appl. Opt.*, **41**( 18), 3725– 3734, doi:[10.1364/AO.41.003725](https://doi.org/10.1364/AO.41.003725) .

[Crossref](#) | [ADS](#) | [PubMed](#) | [Web of Science®](#) | [Google Scholar](#)

---

Mlawer, E. J., and Clough, S. A. ( 1997), On the extension of rapid radiative transfer model to the shortwave region, in *Proceedings of the Sixth Atmospheric Radiation Measurement (ARM) Science Team Meeting*, pp. 223– 226, U.S. Dep. of Energy, Washington, D. C.

[Google Scholar](#)

---

Mlawer, E. J., et al. ( 1997), Radiative transfer for inhomogeneous atmospheres: RRTM, a validated correlated-k model for the longwave, *J. Geophys. Res.*, **102**( D14), 16,663– 16,682, doi:10.1029/97JD00237 .

[Wiley Online Library](#) | [CAS](#) | [ADS](#) | [Web of Science®](#) | [Google Scholar](#)

---

Nee, J. B., et al. ( 1998), Lidar observation of the cirrus cloud in the tropopause at Chung-Li (25°N, 121°E), *J. Atmos. Sci.*, **55**( 12), 2249– 2257, doi:10.1175/1520-0469(1998)055<2249:LOOTCC>2.0.CO;2 .

[Crossref](#) | [ADS](#) | [Web of Science®](#) | [Google Scholar](#)

---

Peter, T., et al. ( 2003), Ultrathin tropical tropopause clouds (UTTCs): I. Cloud morphology and occurrence, *Atmos. Chem. Phys.*, **3**, 1083– 1091, doi:10.5194/acp-3-1083-2003 .

[Crossref](#) | [CAS](#) | [ADS](#) | [Web of Science®](#) | [Google Scholar](#)

---

Pfister, L., et al. ( 2001), Aircraft observations of thin cirrus clouds near the tropical tropopause, *J. Geophys. Res.*, **106**( D9), 9765– 9786, doi:10.1029/2000JD900648 .

[Wiley Online Library](#) | [ADS](#) | [Web of Science®](#) | [Google Scholar](#)

---

Prabhakara, C., et al. ( 1988), Thin cirrus clouds—Seasonal distribution over oceans deduced from Nimbus-4 IRIS, *J. Appl. Meteorol.*, **27**( 4), 379– 399, doi:10.1175/1520-

0450(1988)027<0379:TCCSDO>2.0.CO;2 .

[Crossref](#) | [ADS](#) | [Web of Science®](#) | [Google Scholar](#)

---

Rosenfield, J. E., et al. ( 1998), The impact of subvisible cirrus clouds near the tropical tropopause on stratospheric water vapor, *Geophys. Res. Lett.*, **25**( 11), 1883– 1886, doi:10.1029/98GL01294 .

[Wiley Online Library](#) | [CAS](#) | [ADS](#) | [Web of Science®](#) | [Google Scholar](#)

---

Sassen, K., et al. ( 1989), Optical-scattering and microphysical properties of subvisual cirrus clouds, and climatic implications, *J. Appl. Meteorol.*, **28**( 2), 91– 98, doi:10.1175/1520-

0450(1989)028<0091:OSAMPO>2.0.CO;2 .

[Crossref](#) | [ADS](#) | [Web of Science®](#) | [Google Scholar](#)

---

Schiller, C., et al. ( 2008), Ice water content of Arctic, midlatitude, and tropical cirrus, *J. Geophys. Res.*, **113**, D24208, doi:10.1029/2008JD010342 .

[Wiley Online Library](#) | [CAS](#) | [ADS](#) | [Web of Science®](#) | [Google Scholar](#)

---

Scott, S. G., et al. ( 1990), The Meteorological Measurement System on the NASA ER-2 aircraft, *J. Atmos. Oceanic Technol.*, **7**( 4), 525– 540, doi:10.1175/1520-0426(1990)007<0525:TMMSOT>2.0.CO;2 .

[Crossref](#) | [ADS](#) | [Web of Science®](#) | [Google Scholar](#)

---

Stephens, G. L., et al. ( 1990), The relevance of the microphysical and radiative properties of cirrus clouds to climate and climatic feedback, *J. Atmos. Sci.*, **47**( 14), 1742– 1753, doi:10.1175/1520-



0469(1990)047<1742:TROTMA>2.0.CO;2 .

[Crossref](#) | [ADS](#) | [Web of Science®](#) | [Google Scholar](#)

---

Thomas, A., et al. ( 2002), In situ measurements of background aerosol and subvisible cirrus in the tropical tropopause region, *J. Geophys. Res.*, **107**( D24), 4763, doi:[10.1029/2001JD001385](https://doi.org/10.1029/2001JD001385) .

[Wiley Online Library](#) | [ADS](#) | [Web of Science®](#) | [Google Scholar](#)

---

Toon, O. B., et al. ( 2010), Planning, implementation, and first results of the Tropical Composition, Cloud and Climate Coupling Experiment (TC4), *J. Geophys. Res.*, **115**, D00J04, doi:[10.1029/2009JD013073](https://doi.org/10.1029/2009JD013073) .

[Wiley Online Library](#) | [ADS](#) | [PubMed](#) | [Web of Science®](#) | [Google Scholar](#)

---

Vömel, H., et al. ( 2007), Accuracy of tropospheric and stratospheric water vapor measurements by the cryogenic frost point hygrometer: Instrumental details and observations, *J. Geophys. Res.*, **112**, D08305, doi:[10.1029/2006JD007224](https://doi.org/10.1029/2006JD007224) .

[Wiley Online Library](#) | [CAS](#) | [ADS](#) | [Web of Science®](#) | [Google Scholar](#)

---

Wang, P.-H., et al. ( 1994), Tropical high cloud characteristics derived from SAGE II extinction measurements, *Atmos. Res.*, **34**( 1–4), 53– 83, doi:[10.1016/0169-8095\(94\)90081-7](https://doi.org/10.1016/0169-8095(94)90081-7) .

[Crossref](#) | [Google Scholar](#)

---

Weinstock, E. M., et al. ( 1994), New fast response photofragment fluorescence hygrometer for use on the NASA ER-2 and the Perseus remotely piloted aircraft, *Rev. Sci. Instrum.*, **65**( 11), 3544– 3554, doi:[10.1063/1.1144536](https://doi.org/10.1063/1.1144536) .

[Crossref](#) | [CAS](#) | [ADS](#) | [Web of Science®](#) | [Google Scholar](#)

---

Weinstock, E. M., et al. ( 2009), Validation of the Harvard Lyman- $\alpha$  in situ water vapor instrument: Implications for the mechanisms that control stratospheric water vapor, *J. Geophys. Res.*, **114**, D23301, doi:[10.1029/2009JD012427](https://doi.org/10.1029/2009JD012427) .

[Wiley Online Library](#) | [CAS](#) | [ADS](#) | [PubMed](#) | [Web of Science®](#) | [Google Scholar](#)

---

Winker, D. M., and Trepte, C. R. ( 1998), Laminar cirrus observed near the tropical tropopause by LITE, *Geophys. Res. Lett.*, **25**( 17), 3351– 3354, doi:[10.1029/98GL01292](https://doi.org/10.1029/98GL01292) .

[Wiley Online Library](#) | [ADS](#) | [Web of Science®](#) | [Google Scholar](#)

---

Yang, Q., et al. ( 2010), Radiative impacts of clouds in the tropical tropopause layer, *J. Geophys. Res.*, **115**, D00H12, doi:[10.1029/2009JD012393](https://doi.org/10.1029/2009JD012393) .

[Wiley Online Library](#) | [ADS](#) | [PubMed](#) | [Web of Science®](#) | [Google Scholar](#)

## Citing Literature



[Back to Top](#)



[AGU PUBLICATIONS](#)

[AGU.ORG](#)

[AGU MEMBERSHIP](#)

[RESOURCES](#) ▼

---

[PUBLICATION INFO](#) ▼

---

© 2019 American Geophysical Union

About Wiley Online Library

[Privacy Policy](#)  
[Terms of Use](#)  
[Cookies](#)  
[Accessibility](#)

[Help & Support](#)

[Contact Us](#)

[Opportunities](#)

**Subscription Agents  
Advertisers & Corporate Partners**

Connect with Wiley

**The Wiley Network  
Wiley Press Room**

Copyright © 1999-2019 John Wiley & Sons, Inc. All rights reserved